Computational Engineering and Physical Modeling 1-3 (2018) 46-66

Contents lists available at **CEPM**

Computational Engineering and Physical Modeling

Journal homepage: www.jcepm.com

Modeling of the New Boundary of Reaction Force Based on Particle Collision in the Smoothed Particle Hydrodynamics

L. Wang[1*], P. Wang[2]

1. School of Energy and Power Engineering, Jiangsu University of Science and Technology, Zhenjiang Jiangsu 212003, China
2. School of Mathematics and Information Engineering, Lianyungang Normal College, Lianyungang 222006, China

Corresponding author: *wanglecsi@163.com*

https://doi.org/10.22115/CEPM.2018.141232.1037

ARTICLE INFO

Article history:
Received: 18 July 2018
Revised: 23 August 2018
Accepted: 26 September 2018

Keywords:
Smoothed particle hydrodynamic;
Boundary conditions;
Reaction force;
Particles collision.

ABSTRACT

A new reaction force model of particle collision is built, which is based on the conservation of momentum and the conservation of energy. Combined with weakly compressible smoothed particle hydrodynamics and the artificial compressibility, the new model and a conventional reaction force model of Lennard-Jones is used to simulate the phenomenon of shear driven cavity and the flow around a square cylinder, respectively. For verifying the accuracy of the new model, the DNS method is also used to simulate the flow phenomenon. By comparing and analyzing the calculating results, it can be concluded that: The new reaction force model can effectively prevent particles from unphysically penetrating through the boundary, and the variation of velocity and tangential stress near the boundary can be relatively accurate calculated. The new model helps to enhance the calculation accuracy of smooth particle hydrodynamics (SPH) for the whole flow field, and it has relatively good stability.

How to cite this article: Wang L, Wang P. Modeling of the New Boundary of Reaction Force Based on Particle Collision in the Smoothed Particle Hydrodynamics. Comput Eng Phys Model 2018;1(3):46–66. https://doi.org/10.22115/cepm.2018.141232.1037

1. Introduction

With the development of calculation methods, the meshfree method has heightened people's interest as a new generation of method. The method is viewed as next generation computational techniques [1], it is better than the conventional methods of finite difference method and finite element method in many applications. The smoothed particle hydrodynamics (SPH) are a meshfree method, it was first proposed to study the three –dimensional open space of astrophysics by Lucy [2] and Gingold [3]. Through decades of development, the SPH has broadened and been applied to ocean engineering, medical, solid mechanics, multiphase flow, flow through porous media and so on [4–11]. Especially in the last few years, some investigations of the large eddy simulation and the direct numerical simulation of turbulent flows has been recently done using the SPH method [12,13].

The SPH is a Lagrangian particle method for modeling fluid flows, can be considered as a particle meshfree method. A series of particles are used to describe the state of fluid systems, and some physical quantities of density, pressure, velocity, internal energy and so on are all included in the particle. The particle has no fixed space position, its motion complies with conservation equation.

The core idea of the SPH is interpolation theory, namely the value of arbitrary function at a particle can be expressed as an integral form in support domain of the particle. But when a particle near or on the boundary, its integral can be truncated by the boundary. So the whole flow region cannot completely use the SPH, and the treatment of its boundary condition is more difficult than other number methods. For proper handling the particle on the boundary would have an important effect on the accuracy and stability of the SPH, and it's become a key problem to confine the development of the smoothed particle hydrodynamics [13].

At present, the most remarkable of two boundary methods are repulsive force method and mirror particle method. The most classic of the repulsive force method is based on the molecular force equation of Lennard-Jones [14]. Subsequently, some new algorithms of repulsive force are obtained by Liu G. R. [15], Han. Y. W. [16] and so on. During the repulsive force method, the particles are divided into dummy particles and real particles. The dummy particles are fixed on the boundary, and the fluid medium is discretized into real particles. When the real particle close to the dummy particle, a repulsive force will be applied along the centerline of these two particles, and it can prevent the real particle penetrate through the boundary. The repulsive force method is less affected by the boundary shape, and it is easy realized by using program code. However, for the different flow problems, some different empirical parameters need to be determined in the repulsion force model, and the accuracy of the model will be instability. In addition, the repulsive force generally is artificial force, so it easily results in the momentum nonconservation. However, sometimes the repulsive force is relatively small, and the real particle cannot be effectively prevented penetrate through the boundary. So the mirror particle method is introduced which can be useful to maintain good conservativeness of the boundary [17]. In each evolutionary step, for a real particle near the boundary, a corresponding dummy particle will be placed symmetrically on the outside of the boundary. And the dummy particle has the same density and pressure as the corresponding real particle, but opposite velocity. However, the

mirror particles method is not suitable to model complex shape such as porous medium. Besides, Dalrympl [18] propose that the boundary can be simulated by double rows of particles. The difference between this method and the mirror particles is that the dummy particle is fixed, and it is involved in calculation with real particle. The thickness of the wall can be seen as increased by the dummy particle. This method has proven to have good conservativeness, and it is easier to specify boundary condition.

For internal flow system, the fluid medium offers some force to the wall. According to the idea of SPH, near the boundary, the fluid particle has an impact and collision with the wall, and the wall is the reaction force on the fluid particle. Therefore, in the present study, a new reaction force model of particle-wall collision is built, which is based on the conservation of momentum and the conservation of energy.

In the following, first the SPH method and the governing equations are given. Then the new model of boundary conditions is discussed. At last, the results and discussions including two cases for verification of the new boundary model are presented.

2. Fundamental equations of SPH

The construction method of SPH equations is comprised of integration representation and particle approximation. The integration representation is the most critical first step. The integral representation of function $f(x)$ can be approximated by summing up the values of the nearest neighbor particles.

The integral representation of function $f(x)$ can be defined as:

$$f(x)=\int_{\Omega} f(x')\delta(x-x')dx' \tag{1}$$

where f is a function of space vector $\mathbf{X}$, $\delta(x-x')$ is the Dirac delta function, Ω is the volume of the integral that contains, namely support domain.

The Dirac delta function δ is replaced by smoothing kernel function $w(x-x',h)$, then the kernel function $f(x)$ can be approximate expressed as [19]:

$$\langle f(x)\rangle=\int_{\Omega} f(x')w(x-x',h)dx' \tag{2}$$

where h is the smoothing length, which is used to define the influence area of the s smoothing kernel function w. The angle bracket $\langle\ \rangle$ is approximation operators of the kernel.

By summing up the values of all particles in the support domain, the Eq. 2 can be written in the following form of discretized.

$$
\begin{aligned}
f(x) &= \int_{\Omega} f(x')w(x-x',h)dx' \approx \sum_{j=1}^{N} f(x_j)w(x-x_j,h)\Delta V_j \\
&= \sum_{j=1}^{N} f(x_j)w(x-x_j,h)\frac{1}{\rho_j}(\rho_j \Delta V_j) \\
&= \sum_{j=1}^{N} f(x_j)w(x-x_j,h)\frac{1}{\rho_j}(m_j) = \sum_{j=1}^{N}\frac{m_j}{\rho_j} f(x_j)w(x-x_j,h)
\end{aligned}
\tag{3}
$$

that is

$$
\langle f(x)\rangle = \sum_{j=1}^{N}\frac{m_j}{\rho_j} f(x_j)w_{ij} \qquad w_{ij} = w(x_i - x_j, h) \tag{4}
$$

where ΔV_j is the volume of particle j, ρ_j, m_j is density and mass of particle j, respectively.

By using the divergence theorem, the particle approximation of the spatial derivative of the function $f(x)$ as follows.

$$
\langle \nabla \cdot f(x)\rangle = -\sum_{j=1}^{N}\frac{m_j}{\rho_j} f(x_j)\cdot \nabla w(x-x_j,h) = -\sum_{j=1}^{N}\frac{m_j}{\rho_j} f(x_j)\cdot \nabla w_{ij} \tag{5}
$$

$$
\nabla_i w_{ij} = \frac{x_i - x_j}{r_{ij}}\frac{\partial w_{ij}}{\partial r_{ij}} = \frac{x_{ij}}{r_{ij}}\frac{\partial w_{ij}}{\partial r_{ij}} \tag{6}
$$

where r_{ij} is the distance between the particle i and particle j.

The definition of kernel function is important to the stability of meshless methods [20,21]. In the present study, a quintic interpolating splines is used for smoothing kernel function $w(x-x',h)$. The function is proposed by Morris [22], and it is more approximate to Gaussian kernel function.

$$
w(R,h) = \alpha_d \times \begin{cases} (3-R)^5 - 6(2-R)^5 + 15(1-R)^5 & 0 \le R \le 1 \\ (3-R)^5 - 6(2-R)^5 & 1 \le R < 2 \\ (3-R)^5 & 2 \le R < 2 \\ 0 & R \ge 3 \end{cases} \tag{7}
$$

where α_d is $\frac{120}{h}, \frac{7}{478\pi h^2}, \frac{3}{359\pi h^3}$ for the 1D, 2D and 3D, respectively. R is the relative distance between the particle i and particle j, $R = \frac{\left|\mathbf{x}_i - \mathbf{x}_j\right|}{h}$.

3. The governing equations

Conservation of mass:

$$\frac{d\rho}{dt} = -\rho\nabla\cdot\mathbf{v} \tag{8}$$

Conservation of momentum:

$$\frac{d\mathbf{v}}{dt} = -\frac{1}{\rho}\nabla p + \frac{1}{\rho}\nabla\cdot\tau + \mathbf{F} \tag{9}$$

Conservation of energy:

$$\frac{du}{dt} = -\frac{p}{\rho}\nabla\cdot\mathbf{v} + \frac{1}{\rho}\tau\cdot\nabla\mathbf{v} \tag{10}$$

where ρ is the fluid density, $\mathbf{v} = (v_x, v_y, v_z)$ is velocity vector, p is pressure, $\mathbf{F}$ is body force for unit mass, u is internal energy of fluid element, The viscous stress τ is proportional to the strain rate ε, the proportional coefficient is kinetic viscosity μ:

$$\tau_{ij} = \mu\varepsilon_{ij} = \mu\left(\frac{\partial v_j}{\partial x_i} + \frac{\partial v_i}{\partial x_j} - \frac{2}{3}(\nabla\cdot\mathbf{v})\delta_{ij}\right)\ (i, j = x, y, z) \tag{11}$$

By using above the SPH method, SPH equations of the governing equations are obtained as follows:

$$\frac{d\rho_i}{dt} = \sum_{j=1}^{N} m_j(\mathbf{v}_i - \mathbf{v}_j)\cdot\nabla_i W_{ij} \tag{12}$$

$$\frac{d\mathbf{v}_i}{dt} = -\sum_{j=1}^{N} m_j\left(\frac{p_i}{\rho_i^2} + \frac{p_j}{\rho_j^2}\right)\nabla_i W_{ij} \tag{13}$$

$$\frac{du_i}{dt} = \frac{1}{2}\sum_{j=1}^{N} m_j\left(\frac{p_i}{\rho_i^2} + \frac{p_j}{\rho_j^2}\right)(\mathbf{v}_i - \mathbf{v}_j)\cdot\nabla_i W_{ij} \tag{14}$$

$$\frac{d\mathbf{x}_i}{dt} = \mathbf{v}_i \tag{15}$$

The momentum Eq. 9 shows the coupling relationship between the pressure and the velocity. For the compressible fluid, the motion of particle is driven by pressure gradients. And the pressure change of particle is obtained by density and internal energy through the equation of state equation. However, for the incompressible fluid, the solution of pressure is limited by practical state equation. Therefore, the idea of artificial compressibility is introduced in classical SPH, and the new sate equation is proposed by Monaghan [14], Lee [21], Morris [22] and so on.

$$p = \frac{\rho_0 c^2}{\gamma}((\frac{\rho}{\rho_0})^{\gamma} - 1) \tag{16}$$

$$p = \rho c^2 \tag{17}$$

where γ is a constant coefficient which can be 7, ρ_0 is reference density. c is sound velocity, but it is not the real velocity of sound, or else the time step will be too little. c is normally taken 10 times higher than the maximum fluid velocity [13]. Generally, the Eq. 16 be used to simulate the free surface flow, and the Eq. 17 be used in non-free surface flow.

4. Boundary conditions

As described in the introduction, some new methods are proposed to deal with boundary by the broad masses of scientists, but still have their shortcomings. In the present study, in order to overcome the weakness of empirical parameters determination and momentum nonconservation for the conventional reaction force method, a new reaction force model of particle-wall collision will be built.

4.1. The idea of support domain

The Eq. 1 shows that the value of the function $f(x)$ at point $\mathbf{x}_i = (x_i, y_i, z_i)$ is decided by support domain. That is, the information at the point $\mathbf{x}_i$ is decided by the information for all the points inside this domain. The geometry of support domain is shown in figure 1. Circle with center point $\mathbf{x}_i$, and radius $r = \kappa h$. The distance between $\mathbf{x}_j$ and $\mathbf{x}_i$ inside the domain $r_{ij} = \left|\mathbf{x}_i - \mathbf{x}_j\right|$ must less than radius r. where the κ is a constant coefficient, and the value is 2 in the paper.

4.2. The reaction force model of lennard-jones

Figure 1 shows the interaction relationship of real particle and dummy particle. As described in the introduction, the fluid medium is discretized into a series of real particles, and the dummy particles are fixed on the boundary. When a particle is close to the boundary, its support domain maybe contains some dummy particles. And a repulsive force will be applied to the real particle, it can prevent the real particle penetrate through the boundary.

Based on the molecular force equation of Lennard-Jones, a repulsive force method is proposed by Monaghan as follows.

$$f_{ij} = \begin{cases} D\left[\left(\dfrac{r_0}{r_{ij}}\right)^{n_1} - \left(\dfrac{r_0}{r_{ij}}\right)^{n_2}\right]\dfrac{x_{ij}}{r_{ij}}, & \dfrac{r_0}{r_{ij}} \geq 1 \\ 0, & \dfrac{r_0}{r_{ij}} < 1 \end{cases} \tag{18}$$

where n_1, n_2 are empirical parameters which usually taken as 12 and 4, respectively. D is another empirical parameter, but the value should be chosen to be in the same scale as the square of the largest velocity [13]. r_0 is cutoff distance, and the value is usually approximately equal the initial distance of the particle.

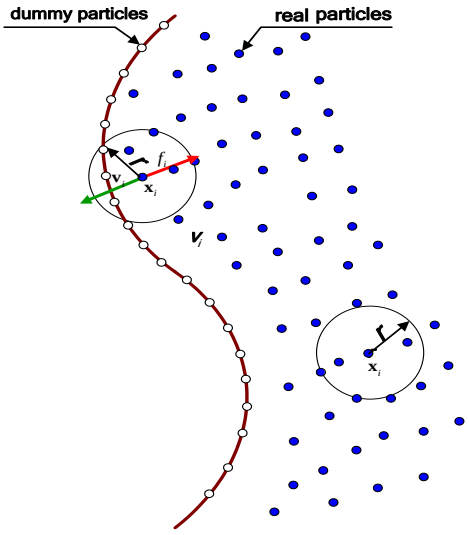

Fig. 1. The interactive relationship of real particle and dummy particle.

The Eq. 18 indicates that not all dummy particles have force on real particle inside the support domain. Only if $r_{ij} < r_0$, the dummy particle have reaction force to real particle.

As the classical model of reaction force, the equation of Lennard-Jones has been widely used. However, if the value of empirical parameter is not inappropriate, the boundary can be unphysically penetrated by real particle. In additional, different empirical parameter setting maybe all could effectively prevent particles from unphysically penetrating through the boundary. But a bigger error in the calculation accuracy will be produced. At the same time, the repulsive force is artificial force, and it easily results in the momentum nonconservation. In order to circumvent those problems, a new repulsive force model is built as follows.

4.3. The reaction force model of particle collision

The new model is similar to the reaction force model of Lennard-Jones. For a support domain of particle i, only if $r_{ij} < r_0$, the dummy particle have reaction force to real particle. But the reaction force is produced by the collision of particle i and particle j, and the collision motion is not considered in the process of SPH calculation.

It is assumed that a real particle i collide with a dummy particle j. Before the collision, the initial momentum and initial angular momentum of real particle i and dummy particle j are labelled as $\mathbf{K}_i, \mathbf{J}_i, \mathbf{K}_j, \mathbf{J}_j$, respectively.

The geometry site of two particles at the moment of collision:

$$\mathbf{r}_0=\mathbf{r}_i+\alpha\mathbf{e}_i=\mathbf{r}_j+\beta\mathbf{e}_j \tag{19}$$

where $\mathbf{r}_0$ is position of collision point. α , β are the coordinate values of collision point, which is based on the coordinate system with the origin at the mass center of particle i and particle j, respectively. $\mathbf{e}$ is basis vector.

The origin of coordinates is moved to the collision point $\mathbf{r}_0$, and then the Eq. 19 gives the following form:

$$\left.\begin{aligned}\mathbf{r}_i&=-\alpha\mathbf{e}_i\\ \mathbf{r}_j&=-\beta\mathbf{e}_j\end{aligned}\right\} \tag{20}$$

After the collision, the new momentum and initial angular momentum of particle i and particle j are labelled as $\mathbf{K}_i', \mathbf{J}_i', \mathbf{K}_j', \mathbf{J}_j'$, respectively. Based on the conservation of momentum, the Eq. (21) can be got:

$$\left.\begin{aligned}\mathbf{K}_i'&=\mathbf{K}_i+\Delta\mathbf{K}_{ij}\\ \mathbf{K}_j'&=\mathbf{K}_j-\Delta\mathbf{K}_{ij}\end{aligned}\right\} \tag{21}$$

where $\Delta\mathbf{K}$ is transfer momentum between the two particles at the moment of collision.

According to the conservation of angular momentum, the following equation can be obtained:

$$\left.\begin{aligned}\mathbf{J}_i'&=\mathbf{J}_i+\alpha\mathbf{e}_i\times\Delta\mathbf{K}_{ij}\\ \mathbf{J}_j'&=\mathbf{J}_j-\beta\mathbf{e}_j\times\Delta\mathbf{K}_{ij}\end{aligned}\right\} \tag{22}$$

By using the conservation of energy, and combining Eq. 22 give the following form:

$$\begin{aligned}\frac{\mathbf{K}_i^2}{2m}+\frac{\mathbf{K}_j^2}{2m}+\frac{\mathbf{J}_i^2}{2\mathbf{I}_c}+\frac{\mathbf{J}_j^2}{2\mathbf{I}_c}&=\frac{(\mathbf{K}_i+\Delta\mathbf{K}_{ij})^2}{2m}+\frac{(\mathbf{K}_j-\Delta\mathbf{K}_{ij})^2}{2m}\\ &+\frac{(\mathbf{J}_i+\alpha\mathbf{e}_i\times\Delta\mathbf{K}_{ij})^2}{2\mathbf{I}_c}+\frac{(\mathbf{J}_j-\beta\mathbf{e}_j\times\Delta\mathbf{K}_{ij})^2}{2\mathbf{I}_c}\end{aligned} \tag{23}$$

where the first term and the second term in the left of equal is the kinetic energy of particle, that is:

$$\frac{1}{2}m\mathbf{v}_i^2+\frac{1}{2}m\mathbf{v}_j^2=\frac{1}{2}\frac{(m\mathbf{v}_i)^2}{m}+\frac{1}{2}\frac{(m\mathbf{v}_j)^2}{m}=\frac{\mathbf{K}_i^2}{2m}+\frac{\mathbf{K}_j^2}{2m}$$

and the third term and the fourth term in the left of equal is the angular kinetic energy of particle, that is:

$$\frac{1}{2}\mathbf{I}_c\omega_i^2+\frac{1}{2}\mathbf{I}_c\omega_j^2=\frac{1}{2}\frac{(\mathbf{I}_c\omega_i)^2}{\mathbf{I}_c}+\frac{1}{2}\frac{(\mathbf{I}_c\omega_j)^2}{\mathbf{I}_c}=\frac{\mathbf{J}_i^2}{2\mathbf{I}_c}+\frac{\mathbf{J}_j^2}{2\mathbf{I}_c}$$

where m, $\mathbf{I}_c$ are the mass and moment of inertia of particle, and the ω_i is angular velocity of particle.

Eq. 23 can be rewritten as:

$$\Delta\mathbf{K}_{ij}\cdot(\underbrace{\frac{\mathbf{K}_i-\mathbf{K}_j}{m}+\frac{\mathbf{J}_i\times\alpha\mathbf{e}_i-\mathbf{J}_j\times\beta\mathbf{e}_j}{\mathbf{I}_c}}_{A})=-\Delta\mathbf{K}_{ij}^2(\frac{1}{m}+\frac{\alpha^2+\beta^2}{2\mathbf{I}_c}) \tag{24}$$

where the A in Eq. 24 is velocity difference of two particles before the collision at the collision point, and denoted by $\Delta\mathbf{u}_{ij}$.

It is assumed the $\Delta\mathbf{K}_{ij}$ and $\Delta\mathbf{u}_{ij}$ with the same direction, and then Eq. (24) can be rewritten as:

$$\Delta\mathbf{K}_{ij}=-\frac{\Delta\mathbf{u}_{ij}}{\frac{1}{m}+\frac{\alpha^2+\beta^2}{2\mathbf{I}_c}} \tag{25}$$

In present study, dummy particle j is fixed in boundary, so the $\beta=0$. And the $\mathbf{I}_c=\frac{1}{10}md_p^2$, where d_p is diameter of particle, it is approximately equal to smoothing length in the paper.

Based on the conservation of momentum, the vector sum of external force on fluid system is equal to the change rate of momentum of fluid systems. So the reaction force to real particle i can be expressed as:

$$\mathbf{f}_i=\Delta\mathbf{K}_{ij}/dt \tag{26}$$

where dt is time step in SPH calculation. And the acceleration complies with Newton's second law:

$$\mathbf{a}=\frac{\mathbf{f}_i}{m_i} \tag{27}$$

where m_i is the mass of particle i.

5. Numerical examples

In order to verify the accuracy of the reaction force model of particle-wall collision, this model is explained and practically verified in two flow phenomenon: shear driven cavity and the flow

around a square cylinder. At the same time, the classical reaction force model of Lennard-Jones and DNS method are used to compare with the new model.

5.1. The shear driven

The structure of the classic shear driven cavity is shown in figure 2. The square cavity is comprised of square vessel, and it is side length is $2.5\times10^{-5}m$. The fluid medium is water, the kinematic coefficient of viscosity and the density are $\upsilon=10^{-6}m^2/s$ and $\rho=10^3kg/m^3$, respectively. It is assumed that the velocity on the topside of square cavity is $v_\tau=10^{-3}m/s$, and other sides keep stationary.

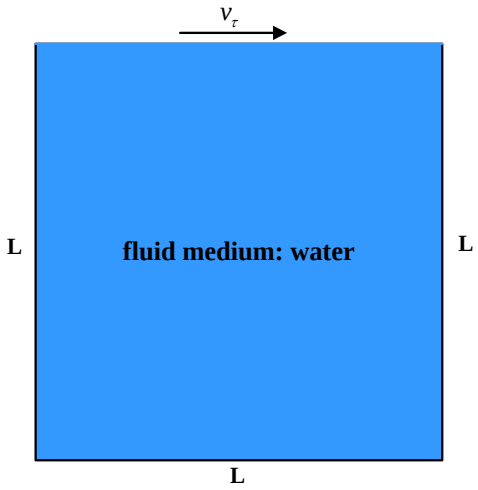

Fig. 2. The structure of classic shear driven cavity.

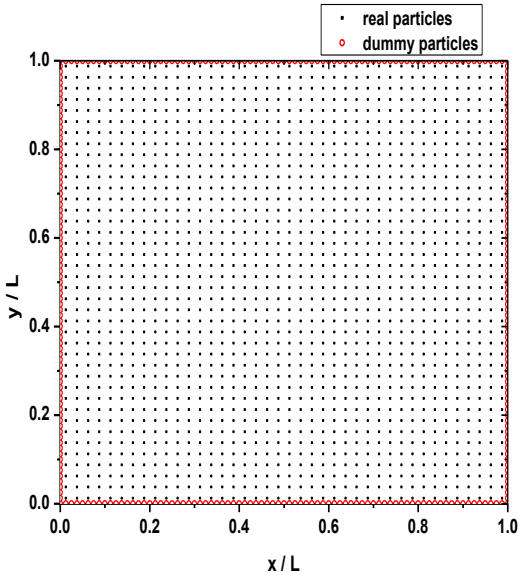

Fig. 3. The initial particle distribution.

The initial particle distribution is shown in figure 3. Comply with the idea of SPH, the water is discretized into 1600 real particles in the square cavity. The initial distance of particles and the smoothing length are 2.5×10^{-5} m. The dummy particles are fixed in the boundary, the initial distance is 2.5×10^{-5} m, and the number is 160. In the whole computing process, a constant time step of 5×10^{-5} s is used, and it takes approximately 3000 steps to reach a steady state.

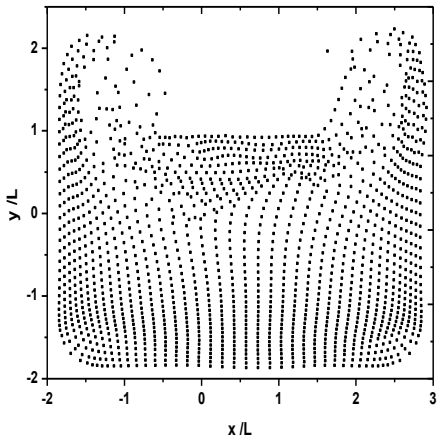

Fig. 4. Particle distributions for no boundary conditions.

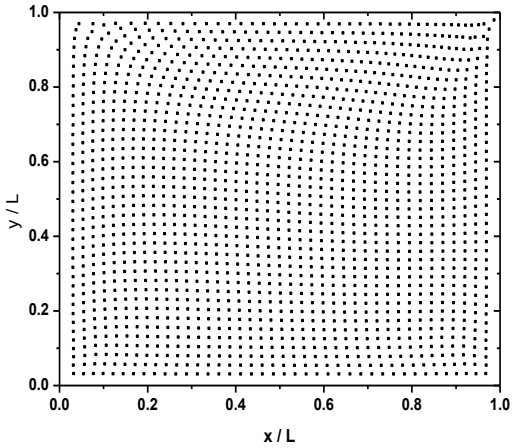

Fig. 5. Particle distributions for new boundary model.

It is effective to prevent real particles from unphysically penetrating through the boundary is a main purpose for appropriate to resolve boundary conditions in SPH. In order to examine the effect of new methods to the boundary, two different conditions are considered in program codes: no dummy particles are fixed in boundary, and the new boundary model is used in the boundary. The particle distribution is shown in figure 4 and figure 5, respectively. It is can be known that, the real particles are free motion comply with conservation law, and its position has exceeded the geometric range of square cavity. However, if the reaction force model of particle-wall collision is used in the boundary, the real particles are limited to inside the square cavity. So, in the present study, the new boundary method can effectively to prevent real particles from unphysically penetrating through the boundary.

Figure 6 shows the velocity vector and streamline of shear driven cavity at steady state. Compare with result of DNS method (as shown in figure 6(c)), a backflow phenomenon are all realized by SPH for the two boundary methods. By using the size of radius vector, it is can conclude that the velocity of particles in the bottom of square cavity is very small. But the vortex is occurred in the corner of square cavity, it is as shown in figure 6(c). That's because in rapidly varied flow, the vortex is formed by the collision of fluid particles. However, the results of SPH methods are shown that the vortexes are not formed in the corner of square cavities, and it is shifted along the clockwise in the square cavity. It is maybe because the real particles in the corner of square cavities, and two side walls could have a reaction force to the real particles at the same time. So the acceleration may be increased too large, and the real particles move from the corner. In addition, classical weakly compressible smoothed particle hydrodynamics method is used to study the water in this paper. Although the method have been verified that it could be used to study the incompressible, but the error of particle displacement still exists, even a phenomenon of particle gathering could occur. So, all of these reasons, the motion of real particles are easy chaotic, and the vortex is moving with the flow of fluid.

The vertical velocities of real particles along the horizontal centerline are shown in figure 7. The result is shown that the variable curve of the reaction force model of particle-wall collision is more corresponding to the DNS method. But an error exists in both sides of the square cavity. It is because that the smoothing length is used to decide the diameter of particles in Eq. (23). When the distance r_{ij} is less than the smoothing length, the reaction force to the real particle i will be bigger. It needs to further improve in the following study. However, for the reaction force model of Lennard-Jones, although it can be effected to prevent real particles from unphysically penetrating through the boundary. But the calculation result is bigger than the result of DNS method, and the error is more obvious. Figure 8 shows the variable curves of horizontal velocities along the vertical centerline. Similarly, the variable curve of the new model has also been more corresponding to the DNS method, and bigger errors exist in the center of square cavity for the reaction force model of Lennard-Jones.

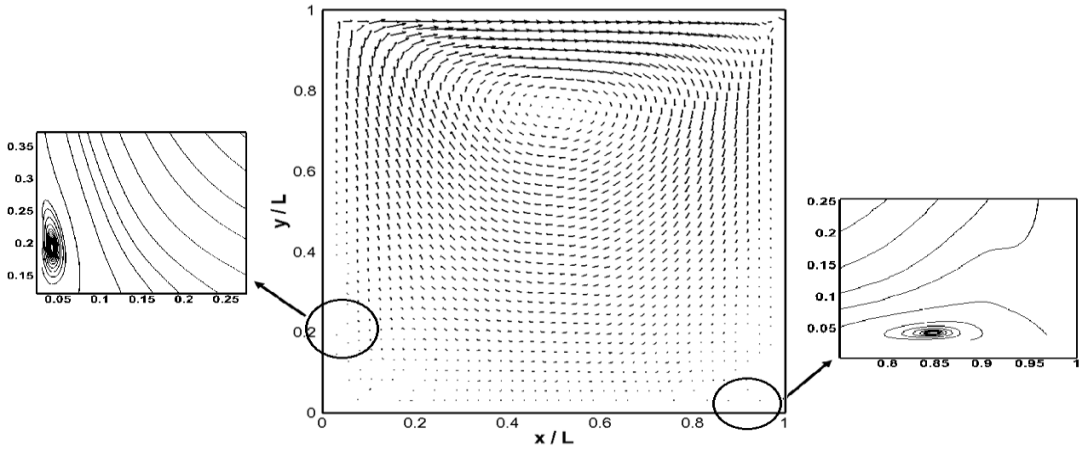

(a) The velocity vector and streamline of real particles in square cavity (the reaction force model of particle-wall collision).

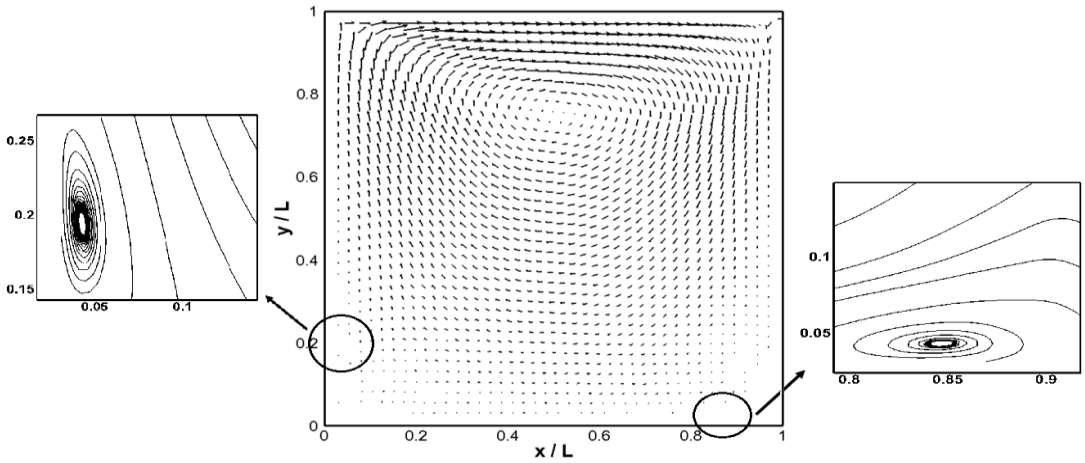

(b) The velocity vector and streamline of real particles in square cavity (the reaction force model of Lennard-Jones).

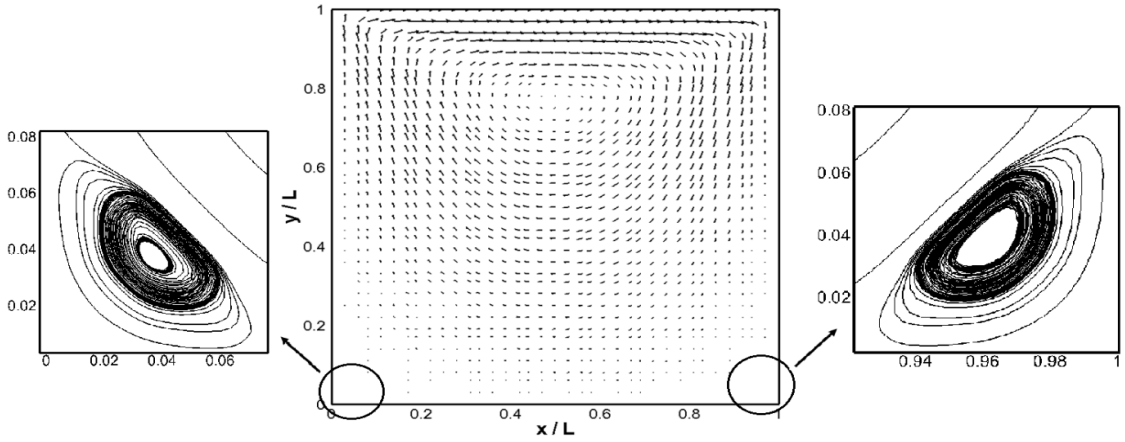

(c) The velocity vector and streamline of real particles in square cavity (the DNS method).

Fig. 6. the velocity vector and streamline of real particles in square cavity.

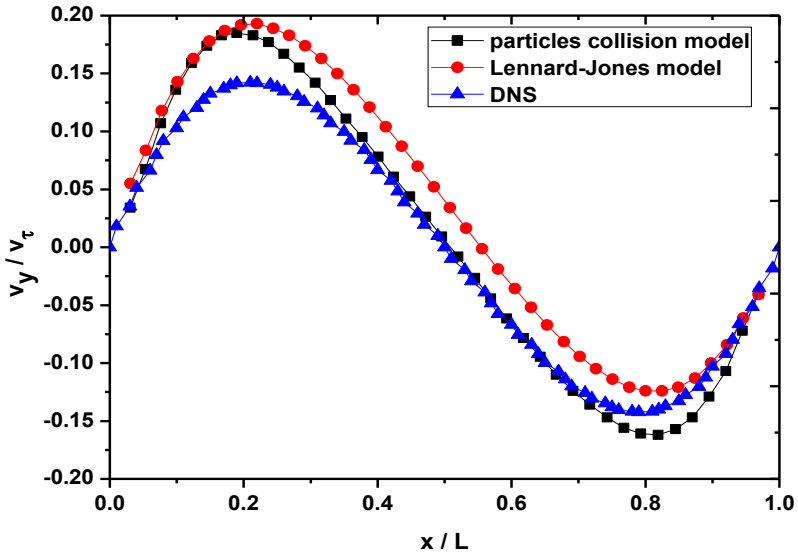

Fig. 7. the variable curves of vertical velocities along the horizontal centerline.

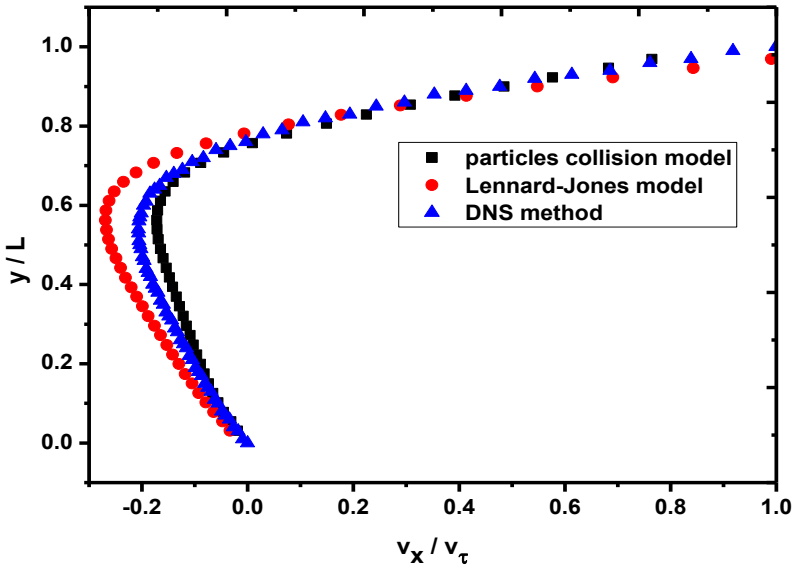

Fig. 8. The variable curves of horizontal velocities along the vertical centerline.

At the same time, the expression of standard error as follows:

$$\sigma = \sqrt{\frac{1}{n}\sum_{i=1}^{n}(x_i - \bar{x})^2} \tag{28}$$

where the n is the number of samples. x_i is sample data, $\bar{x}$ is average of sample data.

Table 1
The standard errors of vertical velocities and horizontal velocities.

Simulation method	standard error v_y / v_τ	standard error v_x / v_τ
The model of particle collision	0.013927	0.018719
The model of Lennard-Jones	0.014272	0.033759

With the velocity value of the DNS in figure 7 and figure 8 as standard, the standard errors of vertical velocities and horizontal velocities of SPH for two boundary methods are shown in Table 1. The results are shown that the standard error of the new method is obviously less than the method of Lennard-Jones's. So, in the present study, the reaction force model of particle-wall collision can help to improve the calculation accuracy of the SPH in some extent.

5.2. Flow around a square cylinder

The fluid flow around a square cylinder is a common phenomenon in nature and engineering. It includes the transition of shear layer, the vortex shedding of periodicity, the formation and development of wake, and so on. Because of the complexity of flow phenomenon, it is usually used as standard examples to test the number simulation of flow. A structure of flow around a

square cylinder is shown in Figure 9. The side length of square cylinder is L, the length of the whole space is 20L. The fluid medium is water, and it is located in the front of space, the area is 5L×5L.

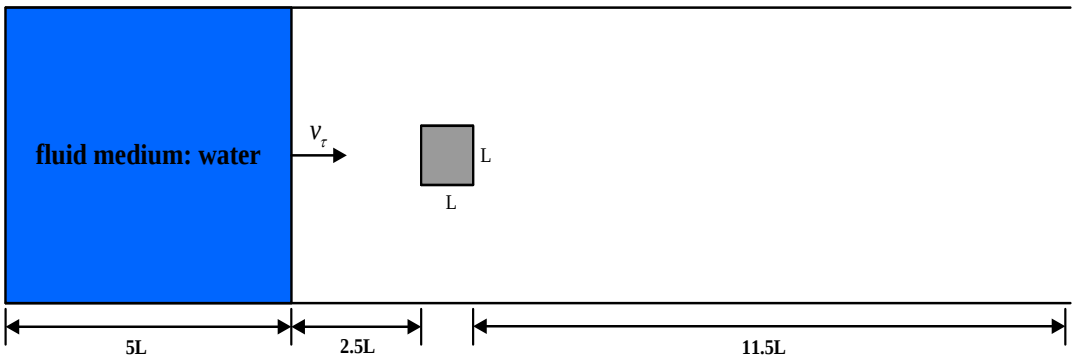

Fig. 9. The structure of flow around a square cylinder.

The water is discretized into 1600 real particles, the initial distance of particles and the smoothing length are 2.5×10^{-5} m. The dummy particles are fixed in upper, lower and left side of the wall. The periodic boundary condition is used in the right side of the wall. The initial distance of dummy particles is 2.5×10^{-5} m, and the number is 785. The test example is investigated by the reaction force model of particle-wall collision, the reaction force model of Lennard-Jones and DNS method, respectively. The flow at Reynolds 150, it is based on the characteristic length of the square cylinder and the inlet velocity. In the whole computing process, a constant time step of 5×10^{-5} s is used. And the simulation time is 8s, it takes 160000 steps.

The real particles distributions for the new boundary model and the classical model of Lennard-Jones at 8s are shown in figure 10(a) and figure 10(b), respectively. It is can be found that the two methods are all successful to prevent real particles from unphysically penetrating through the boundary. The real particles flow around the square cylinder is formed, and the rear stagnation region is occurring behind the square cylinder. It is shown as the blue zone in the figure 10.

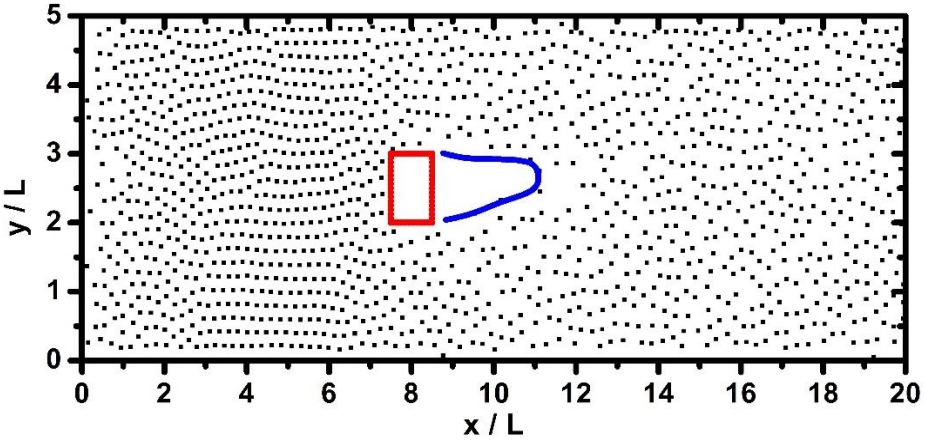

(a) Particles distributions for the new boundary model.

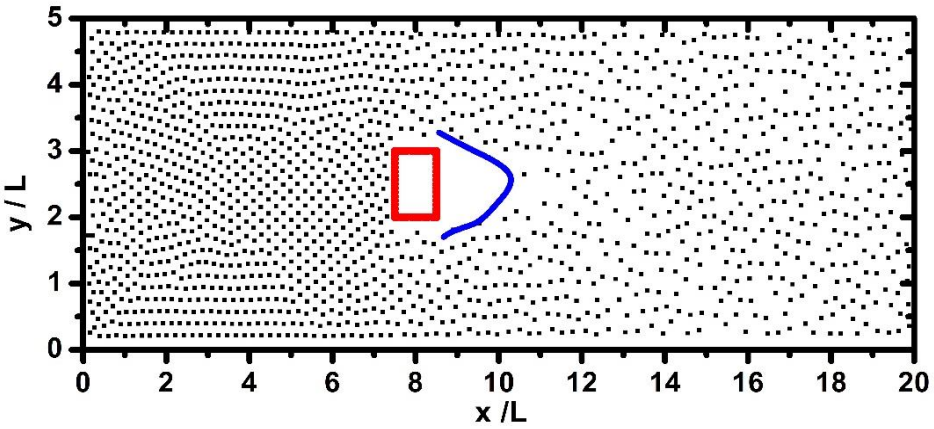

(b) Particles distributions for the boundary model of Lennard-Jones.

Fig. 10. Particles distributions at t=8s.

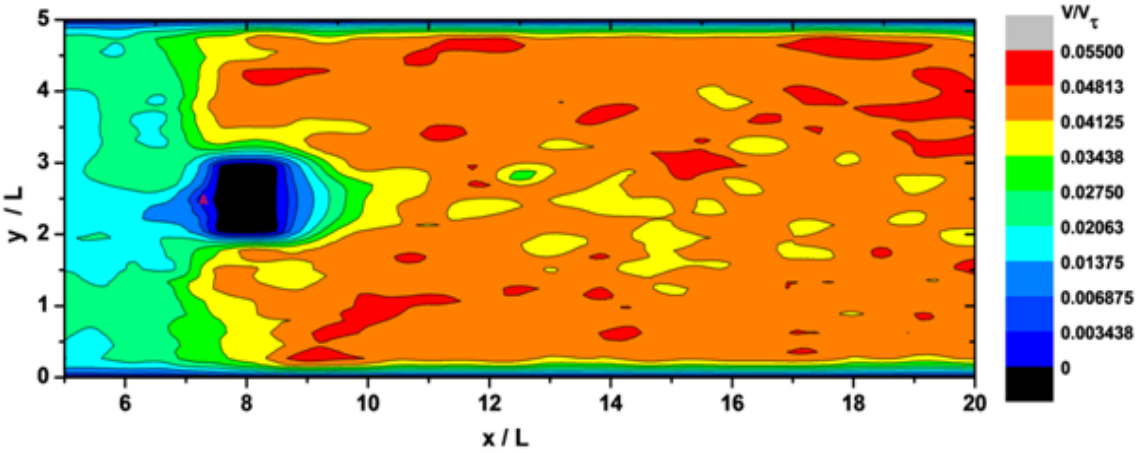

(a) The reaction force model of particle-wall collision.

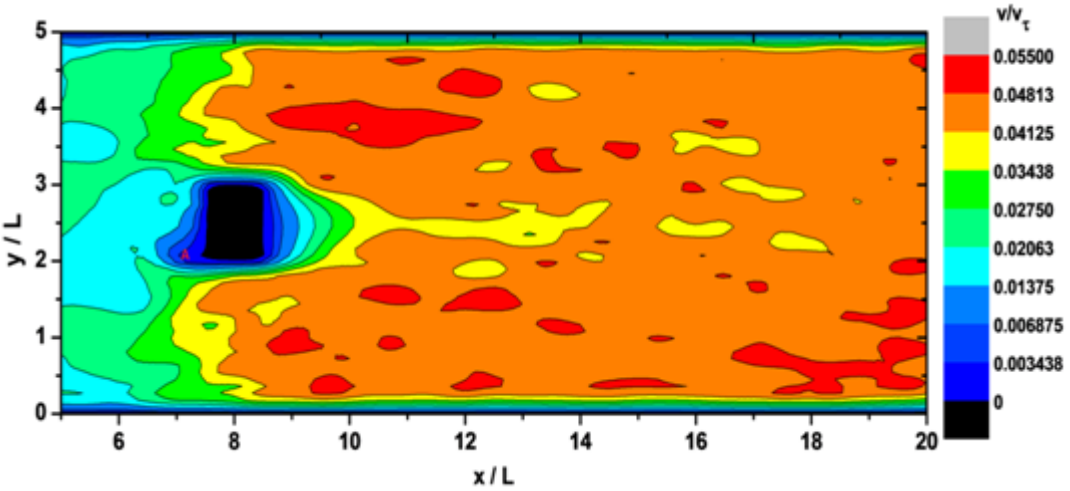

(b) The reaction force model of Lennard-Jones.

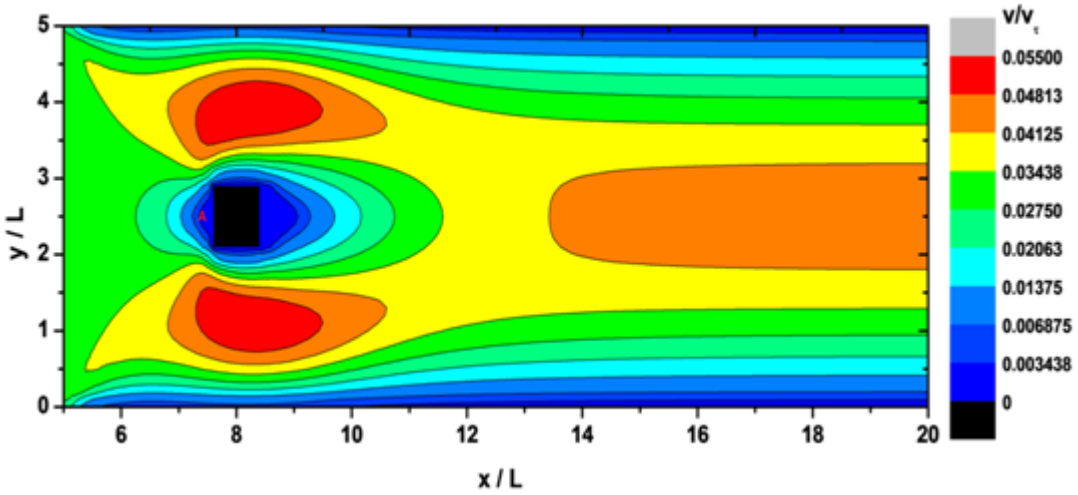

(c) DNS method.

Fig. 11. comparison diagram of velocity contour at t=8s for the different methods.

The velocity contour behind the square cylinder at t=8s are shown in figure 11. The value of velocity gradually reduces to 0 before the fluid reaches the square cylinder. It is as shown the point A in figure, and the point is forward stagnation point. For the result of classic Lennard-Jones model as shown in figure 11(b), it is compared with the result of DNS method (Figure 11(c)), it is can be found that the position of forward stagnation point is far away from square cylinder, and it is located in the bottom of square cylinder. However, for the result of the new boundary model as shown in figure 11(a), the position of forward stagnation point is good agreement with the result of DNS. After the fluid flow through the forward stagnation point, it is along the side of a square cylinder to flow. The velocity first increases gradually, and then the fluid flow into the rear stagnation region. As can be known from the figure 11(c), the low velocity area ($v/v_\tau < 0.03175$) is bigger than the results of SPH for the two boundary methods. It is because the DNS method is based on the continuity of fluid, and the tangential stress is a main influencing factor in the velocity variation of laminar fluid near the boundary. But in the SPH calculation, in addition to considering the tangential stress, the wall has a reaction force to the particles is existed. It has increased the momentum exchange, and the velocity gradient is bigger near the boundary.

At the same time, the figure 11(a) and the figure 11(b) reveals that a big velocity gradient is exited near the boundary for the SPH method, that is, the tangential stress will be bigger. A variation curves of tangential stress along the vertical centerline x/L=12 are shown in figure 12. It is can be known that the tangential stress near the boundary is bigger than fully developed regional. But the tangential stress is calculated by the classic Lennard-Jones model, which is almost 5 times of the result of DNS method. Although an error exists in the calculation result of the new boundary method, but it is relatively smaller. It demonstrates that the reaction force is obtained by using the new boundary model is more reasonable.

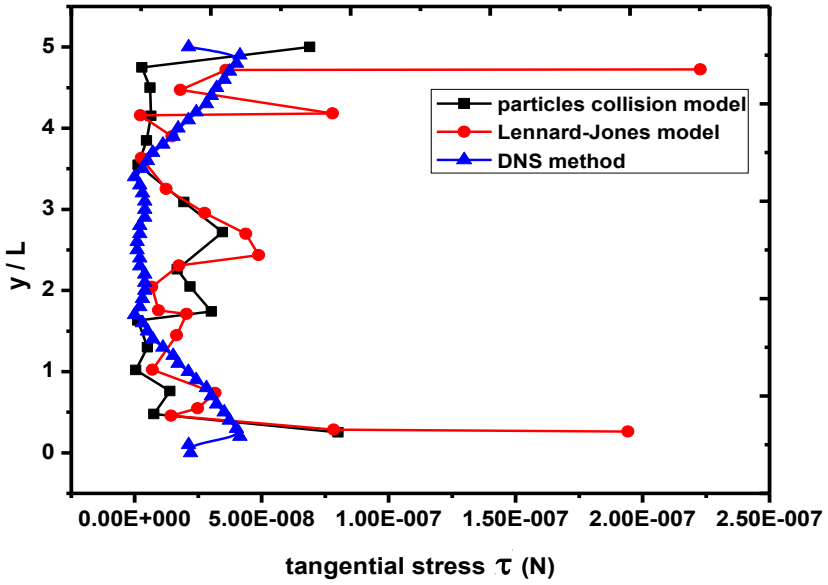

Fig. 12. the variation curves of tangential stress along the vertical centerline x/L=12.

Through above analysis, it is can be known that the appropriate empirical parameters can help the model of Lennard-Jones to successfully to prevent real particles from unphysically penetrating through the boundary, but a bigger error is exit near the boundary. And the reaction force model of particle-wall collision can help to improve the calculation accuracy.

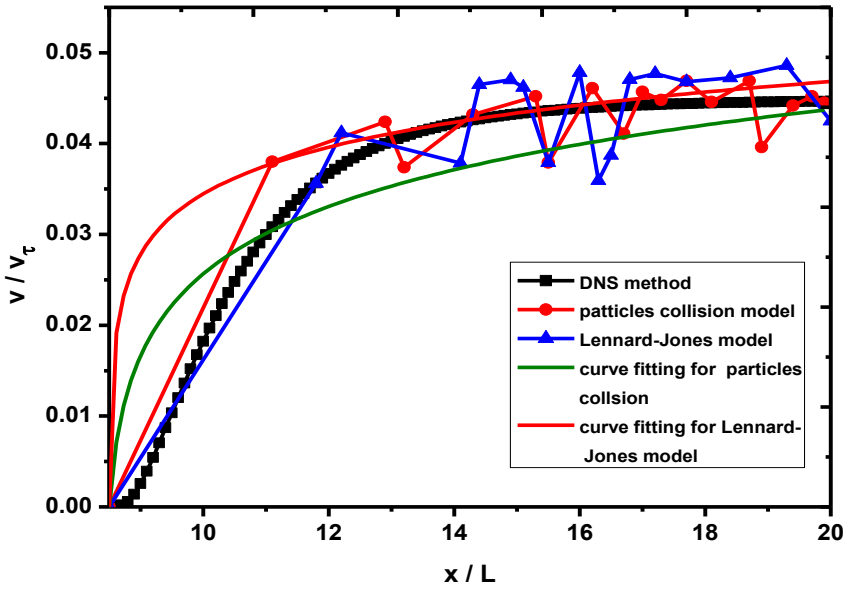

Fig. 13. the velocity variation and fitting curve along the horizontal centerline y/L=2.5.

The velocity recovery is a problem, which is always exit in the number simulation of the flow around a square cylinder. The curves of velocity variation along the horizontal centerline y/L=2.5 are shown in figure 13. It is can be known that the trend of velocity for SPH method is similar with the result of DNS method, but the fluctuation of velocity variation is larger. Because of the meshfree technology is used in SPH, the data are obtained by according the trajectory of a particle, and it is not by using the mesh nodes. The number of particles is a limited quantity in this example, so the curve of velocity variation is larger. So, by using the nonlinear fitting, the discrete points are fitted to functional Eq. 29 and Eq. 30 for the new boundary model and the classical Lennard-Jones model, respectively.

$$\frac{v}{v_\tau} = 0.03351 + 0.00476\ln(\frac{x}{L} - 8.49912) \tag{29}$$

$$\frac{v}{v_\tau} = 0.03031 + 0.00666\ln(\frac{x}{L} - 8.48941) \tag{30}$$

Table 2
The error value of nonlinear fitting.

Simulation Method	Adjusted R-Square	Mean Square Error	Residual
The model of particle collision	0.93721	7.1032×10^{-6}	1.06548×10^{-4}
The model of Lennard-Jones	0.85914	1.86126×10^{-5}	2.60577×10^{-4}

The adjusted R-Square, the mean square error and the residual of fitting results are shown in table 2. Because the adjusted R-Square for the two methods are all approximate equal 1, and the mean square error and the residual are all quite small, so the fitting equations have better reliability. The fitting curves are shown in Figure 13. Because of a big velocity gradient is exited behind the square cylinder for the SPH method, so the velocity is recovering quickly, and it is shown in the fitting curves. However, it is different from the result of DNS method. The calculation result of the SPH method has a good agreement with the result of DNS in x/L>13. But the result of Lennard-Jones model is shown that the curve of velocity is still growing in x/L>18, and the error gradually increasing. On the contrary, the result of new model still has a good agreement with the result of DNS in x/L>13.

Table 3
The standard errors of velocity recovery.

Simulation Method	The model of particle-wall collision	The model of Lennard-Jones
Standard Error	0.000273	0.000522

With the velocity value of DNS as standard, by using the Eq. 25, the standard errors of velocity recovery of SPH for two boundary methods in x/L>13 are shown in Table 3. The standard error of the new boundary model is also less than the method of Lennard-Jones's.

So, for the boundary conditions are treated properly, and it has an important influence on the calculation results of SPH. In the present study, the reaction force model of particle-wall collision has relatively high accuracy. But because of classical weakly compressible smoothed particle hydrodynamics method in this paper, so some errors still exist in the calculation results.

6. Conclusion

In the present study, it is based on the classic of weakly compressible smoothed particle hydrodynamics method, and by using the conservation of momentum and conservation of energy, the new reaction force model is built. The new model and the classic reaction force model of Lennard-Jones are used in the shear driven cavity and the flow around a square cylinder. With the result of DNS as standard, by comparing and analyzing the calculating results, it can be concluded that:

(1) The more reasonable of reaction force can be obtained by using the new boundary model. And the reaction force can effectively prevent particles from unphysically penetrating through the boundary.

(2) The variation of particle velocity and the tangential stress can be calculated by using the new boundary model. It helps to improve the calculation accuracy of the SPH in some extent.

(3) The new boundary model can be sustained long time steps to run by program, and it has a good stability.

(4) The reaction force model of particle-wall collision can overcome the weakness of empirical parameters determination and momentum nonconservation for the classical reaction force model of Lennard-Jones.

Acknowledgements

We gratefully acknowledge the financial support of the National Science Foundation of China (21406095).

References

[1] Daxini SD, Prajapati JM. A Review on Recent Contribution of Meshfree Methods to Structure and Fracture Mechanics Applications. Sci World J 2014;2014:1–13. doi:10.1155/2014/247172.

[2] Lucy LB. A numerical approach to the testing of the fission hypothesis. Astron J 1977;82:1013. doi:10.1086/112164.

[3] Gingold RA, Monaghan JJ. Smoothed particle hydrodynamics: theory and application to non-spherical stars. Mon Not R Astron Soc 1977;181:375–89. doi:10.1093/mnras/181.3.375.

[4] Altomare C, Crespo AJC, Domínguez JM, Gómez-Gesteira M, Suzuki T, Verwaest T. Applicability of Smoothed Particle Hydrodynamics for estimation of sea wave impact on coastal structures. Coast Eng 2015;96:1–12. doi:10.1016/j.coastaleng.2014.11.001.

[5] Soutter J, Hamilton N, Russell P, Russell C, Bushby K, Sloper P, et al. The Golden Freeway: a preliminary evaluation of a pilot study advancing information technology as a social intervention

for boys with Duchenne muscular dystrophy and their families. Heal Soc Care Community 2004;12:25–33. doi:10.1111/j.1365-2524.2004.00465.x.

[6] Nguyen MT, Aly AM, Lee S-W. A numerical study on unsteady natural/mixed convection in a cavity with fixed and moving rigid bodies using the ISPH method. Int J Numer Methods Heat Fluid Flow 2018;28:684–703. doi:10.1108/HFF-02-2017-0058.

[7] Aly AM. Modeling of multi-phase flows and natural convection in a square cavity using an incompressible smoothed particle hydrodynamics. Int J Numer Methods Heat Fluid Flow 2015;25:513–33. doi:10.1108/HFF-05-2014-0161.

[8] Basser H, Rudman M, Daly E. SPH modelling of multi-fluid lock-exchange over and within porous media. Adv Water Resour 2017;108:15–28. doi:10.1016/j.advwatres.2017.07.011.

[9] Kunz P, Zarikos IM, Karadimitriou NK, Huber M, Nieken U, Hassanizadeh SM. Study of Multi-phase Flow in Porous Media: Comparison of SPH Simulations with Micro-model Experiments. Transp Porous Media 2016;114:581–600. doi:10.1007/s11242-015-0599-1.

[10] Mayrhofer A, Laurence D, Rogers BD, Violeau D. DNS and LES of 3-D wall-bounded turbulence using Smoothed Particle Hydrodynamics. Comput Fluids 2015;115:86–97. doi:10.1016/j.compfluid.2015.03.029.

[11] Di Mascio A, Antuono M, Colagrossi A, Marrone S. Smoothed particle hydrodynamics method from a large eddy simulation perspective. Phys Fluids 2017;29:035102. doi:10.1063/1.4978274.

[12] Ni W, Lu L, Fang J, Moulinec C, Yao Y. Direct numerical simulation of turbulent channel flow with spanwise alternatively distributed strips control. Mod Phys Lett B 2018;32:1840004. doi:10.1142/S0217984918400043.

[13] Liu, G. R. and Liu, M. B., Smoothed Particle Hydrodynamics: A meshfree particle method, Word Scientific Publishing Co, Pte. Ltd. 2003.

[14] Monaghan JJ. Simulating Free Surface Flows with SPH. J Comput Phys 1994;110:399–406. doi:10.1006/jcph.1994.1034.

[15] Liu GR, GU YT. A Local Radial Point Interpolation Method (LRPIM) for Free Vibration Analyses of 2-D Solids. J Sound Vib 2001;246:29–46. doi:10.1006/jsvi.2000.3626.

[16] Hong-Fu HY-WQ, Wei-Ran ZJ-LG. A new repulsive model for solid boundary condition in smoothed particle hydrodynamics [J]. Acta Phys Sin 2013;4.

[17] Cummins SJ, Rudman M. An SPH Projection Method. J Comput Phys 1999;152:584–607. doi:10.1006/jcph.1999.6246.

[18] Dalrymple RA, Knio O. SPH Modelling of Water Waves. Coast. Dyn. ’01, Reston, VA: American Society of Civil Engineers; 2001, p. 779–87. doi:10.1061/40566(260)80.

[19] Liu MB, Liu GR, Zong Z. An Overview on Smoothed Particle Hydrodynamics. Int J Comput Methods 2008;05:135–88. doi:10.1142/S021987620800142X.

[20] Morris JP. Analysis of smoothed particle hydrodynamics with applications. Monash University Australia; 1996.

[21] Lee E-S, Moulinec C, Xu R, Violeau D, Laurence D, Stansby P. Comparisons of weakly compressible and truly incompressible algorithms for the SPH mesh free particle method. J Comput Phys 2008;227:8417–36. doi:10.1016/j.jcp.2008.06.005.

[22] Morris JP, Fox PJ, Zhu Y. Modeling Low Reynolds Number Incompressible Flows Using SPH. J Comput Phys 1997;136:214–26. doi:10.1006/jcph.1997.5776.